Title: Photoelectrochemical and thermal characterization of aromatic hydrocarbons substituted with a dicyanovinyl unit

Author: Sonia Kotowicz, Danuta Sęk, Sławomir Kula, Aleksandra Fabiańczyk, Jan Grzegorz Małecki, Ewa Schab-Balcerzak i in.

Citation style: Kotowicz Sonia, Sęk Danuta, Kula Sławomir, Fabiańczyk Aleksandra, Małecki Jan Grzegorz, Schab-Balcerzak Ewa i in. (2020). Photoelectrochemical and thermal characterization of aromatic hydrocarbons substituted with a dicyanovinyl unit. "Dyes and Pigments" 2020, art no 108432, doi 10.1016/j.dyepig.2020.108432

Photoelectrochemical and thermal characterization of aromatic hydrocarbons substituted with a dicyanovinyl unit

Sonia Kotowicz[1], Danuta Sęk[2], Sławomir Kula[1], Aleksandra Fabiańczyk[1], Jan Grzegorz Małecki [2], Paweł Gnida [2], Sebastian Maćkowski[3], Mariola Siwy[2], Ewa Schab-Balcerzak[1,2]*

[1] *Institute of Chemistry, University of Silesia, 9 Szkolna Str., 40-006 Katowice, Poland*

[2] *Centre of Polymer and Carbon Materials, Polish Academy of Sciences, 34 M. Curie-Sklodowska Str., 41-819 Zabrze, Poland*

[3]*Institute of Physics, Faculty of Physics, Astronomy and Informatics, Nicolaus Copernicus University, 5 Grudziadzka Str., 87-100 Torun, Poland*

Abstract: Seven aromatic hydrocarbons bearing a dicyanovinyl unit were prepared to determine the relationship between both the number of aromatic rings and location of acceptor substituent on their thermal and optoelectronic properties. Additionally, the density functional theory calculations were performed. The obtained compounds showed temperatures of the beginning of thermal decomposition in the range of 137 – 289 °C, being above their respective melting points found between 88 and 248 °C. They were electrochemically active and showed *quasi*-reversible reduction process (except for 2-(phen-1-yl)methylene)malononitrile). Electrochemically estimated energy band gaps were below 3.0 eV, in the range of 2.10 – 2.50 eV. The absorption and emission spectra were recorded in $CHCl_3$ and NMP and in solid state. All compounds strongly absorbed radiation with absorption maximum ranging from 307 to 454 nm ascribed to the intramolecular charge transfer between the donor and acceptor units. The aromatic hydrocarbons were luminescent in all investigated media and exhibited higher photoluminescence quantum yields in the solid state due to the aggregation induced emission phenomena. Electroluminescence ability of selected compounds was tested in a diode with guest-host configuration. Additionally, the selected compound together with a commercial N719 was applied in the dye-sensitized solar cell.

Keywords: Malononitrile derivatives, luminescence, electrochemistry, dye-sensitized solar cells

1. Introduction

Organic molecules consisting of donor and acceptor moieties connected through π-conjugated linkages, where the intramolecular charge transfer (ICT) can occur, are widely investigated due to the possibility of applications in optoelectronic devices, such as organic light-emitting diodes (OLEDs), photovoltaic (PV) cells and organic field-effect transistors (OFETs) [1-4]. Aromatic malononitrile derivatives due to their push-pull structure are widely investigated as materials exhibiting interesting optoelectronic properties. They may show for instance desirable aggregation induced emission phenomenon (AIE). Much research have been devoted to their synthesis using different catalysts. The synthetic approach for preparation of aromatic malononitrile derivatives presented in this work has been reported in literature [5-15]. However, thermal, UV-vis, luminescence and electrochemical properties of the obtained compounds have not been systematically studied.

Lin et al. [16] investigated 2-(naphthalene-1-ylmethylene)malononitrile as ligand for CN^- anion detection in water and showed its excellent sensitivity and selectivity with detection limit as low as $1.6 \cdot 10^{-7}$ mol/L. Turpaev et al. [17] described structure-activity relationship of 2-[(phen-1-yl)methylene]malononitrile and 2-[(naphthalen-2-yl)methylene]malononitrile as activators of cell resistance to oxidative stress and modulators of multiple signaling pathways. Kristmamoorthy et al. [18] studied isomerization of malononitrile derivatives with naphthalene units under irradiation ($\lambda_{ex} \succcurlyeq$ above 340 nm) at -196°C. They found that 2-[(naphthalen-2-yl)methylene]malononitrile showed negligible changes upon irradiation at -196°C. Precisely controlled nanowires and microwires with lengths reaching several millimeters were prepared by casting 2-(anthracene-9-yl)methylenemalononitrile from CH_2Cl_2 solution. The nanowires and microwires allowed for construction of a photoswiching device [19]. Kathiraven et al. [20] synthesized a series of compounds, in which pyrene was substituted with various groups, including also dicyanovinylene unit as sensitizers for dye-sensitized solar cells (DSSC). Paramaguru et al. [21] also reported pyrene dyes with various electron withdrawing groups, among them 2-[(pyren-1-yl)methylene)malononitrile was presented and their optical properties in various solvents were measured. Binding affinity with TiO_2, and its dependence on the structure of the compounds was investigated. Experimental results were combined with theoretical calculations. Breffke et al. [22] studied malononitrile derivatives bearing naphthalene units in order to determine their potential utility as fluidity probes. Katritzky et al. [23] synthesized compounds with dicyanovinylene unit with phenyl, α-naphthyl, anthracene, phenanthrene and pyrene moieties, and investigated their optical properties (UV-vis, PL) in various solvents (toluene, diethyl ether, 1,4-dioxane, THF, ethyl acetate, CH_2Cl_2, DMF and CH_3CN).

Intermolecular charge transfer properties and photoluminescence ability were discussed in relation to the solvents polarity.

In this paper the selected properties of seven aromatic malononitrile derivatives with phenyl, biphenyl, α-naphthyl, β-naphthyl, anthracene, phenanthrene and pyrene moieties are presented. Even though these compounds have been presented in the literature, their optical properties were not measured in the solid state and their electroluminescence ability was not examined. The aim of this work focuses on the relationship between their aromatic part structure and properties important for applications in optoelectronics. Geometric structures and frontier molecular orbitals of the studied molecules, and the UV-Vis and PL spectra were calculated using DFT and TD-DFT methods. Selected compounds, that is, 2-((1,1'-biphenyl)-4-yl-methylene)malononitrile and 2-((phenanthren-9-yl)methylene)malononitrile were tested in light emitting diodes with guest-host configuration. Additionally, the compound which showed the highest light harvesting efficiency (LHE), that is, 2-((pyren-1-yl)methylene)malononitrile was tested with N719 in DSSC device.

2. Experimental section

All chemicals utilized in this work were purchased from Sigma Aldrich (Merck). The aluminum oxide 90 active neutral (CAS 1344-28-1) was purchased from Merck.

Characterization methods, films, OLED and DSSC preparations and photovoltaic measurements are described in Supplementary Material.

2.1. Typical Procedure for the synthesis of malononitrile derivatives

Into a solution of malononitrile (8.00 mmol) in methylene chloride (20 mL), aluminum trioxide (800 mg) and the appropriate aldehyde (4.00 mmol) were added. The reaction mixture was stirred at room temperature for 24 h. After this time, the crude product was purified using column chromatography (SiO_2, CH_2Cl_2). All compounds were prepared according to the method described in our previous paper [24].

2-((phen-1-yl)methylene)malononitrile (1)

White powder. **Yield:** 89%. **^{1}H NMR (400 MHz, $CDCl_3$) δ** 7.91 (d, *J* = 7.5 Hz, 2H), 7.78 (s, 1H), 7.66 – 7.61 (m, 1H), 7.55 (t, *J* = 7.6 Hz, 2H). **^{13}C NMR (100 MHz, $CDCl_3$) δ** 159.91, 134.63, 131.16, 130.78, 129.73, 113.76, 112.62, 83.20. **FT-IR** (KBr, *v*, cm^{-1}): 3031 (C-H aromatic); 2223 (-C≡N), 1591 (C=C); 1567 (C-C stretching in the aromatic ring); 1186 (C-N

stretching); 677 (C-N deformation). **Anal. Calcd** for $C_{10}H_6N_2$ (154.16 g/mol): C, 77.91; H, 3.92; N, 18.17; Found: C, 77.90; H, 4.11; N, 17.00. DSC T_m = 88˚C.

2-((1,1'-biphenyl)-4-yl-methylene)malononitrile (2)

Light yellow-green powder. **Yield:** 73%. **^{1}H NMR (400 MHz, $CDCl_3$) δ** 8.00 (d, *J* = 8.3 Hz, 2H), 7.81 – 7.73 (m, 3H), 7.68 – 7.61 (m, 2H), 7.53 – 7.41 (m, 3H). **^{13}C NMR (100 MHz, $CDCl_3$) δ** 159.33, 147.46, 139.00, 131.51, 129.91, 129.30, 129.13, 128.14, 127.36, 114.03, 112.93, 82.12. **FT-IR** (KBr, *v*, cm^{-1}): 3063 (C-H aromatic); 2225 (-C≡N), 1604 (C=C); 1573 (C-C stretching in the aromatic ring); 1197 (C-N stretching); 689 (C-N deformation). **Anal. Calcd** for $C_{16}H_{10}N_2$ (230.26 g/mol): C, 83.46; H, 4.38; N, 12.17; Found: C, 83.13; H, 4.68; N, 12.11. DSC T_m = 144˚C.

2-((naphthalen-1-yl)methylene)malononitrile (3)

Yellow powder. **Yield:** 87%. **^{1}H NMR (400 MHz, $CDCl_3$) δ** 8.66 (s, 1H), 8.28 (d, *J* = 7.3 Hz, 1H), 8.12 (d, *J* = 8.2 Hz, 1H), 7.96 (d, *J* = 8.3 Hz, 2H), 7.72 – 7.60 (m, 3H). **^{13}C NMR (100 MHz, $CDCl_3$) δ** 157.65, 134.97, 133.81, 131.31, 129.59, 128.69, 128.62, 127.78, 127.43, 125.52, 122.48, 113.81, 112.59, 85.59. **FT-IR** (KBr, *v*, cm^{-1}): **FTIR** (KBr, *v*, cm^{-1}): 3028 (C-H aromatic); 2227 (-C≡N), 1590 (C=C); 1566 (C-C stretching in the aromatic ring); 1244 (C-N stretching); 778 (C-N deformation). **Anal. Calcd** for $C_{14}H_8N_2$ (204.27 g/mol): C, 82.33; H, 3.92; N, 13.72; Found: C, 82.48; H, 4.16; N, 13.90. DSC T_m = 170˚C.

2-((naphthalen-2-yl)methylene)malononitrile (4)

Light yellow-green powder. **Yield:** 84%. **^{1}H NMR (400 MHz, $CDCl_3$) δ** 8.29 (s, 1H), 8.08 (dd, *J* = 8.7, 1.8 Hz, 1H), 7.96 (d, *J* = 8.4 Hz, 2H), 7.92 – 7.86 (m, 2H), 7.71 – 7.66 (m, 1H), 7.64 – 7.59 (m, 1H). **^{13}C NMR (100 MHz, $CDCl_3$) δ** 159.69, 136.07, 134.34, 132.86, 130.07, 129.79, 129.78, 128.77, 128.16, 127.86, 124.45, 114.07, 112.95, 82.66. **FT-IR** (KBr, *v*, cm^{-1}): **FTIR** (KBr, *v*, cm^{-1}): 3031 (C-H aromatic); 2226 (-C≡N), 1623 (C=C); 1585 (C-C stretching in the aromatic ring); 1183(C-N stretching); 743 (C-N deformation). **Anal. Calcd** for $C_{14}H_8N_2$ (204.27 g/mol): C, 82.33; H, 3.95; N, 13.72; Found: C, 82.60; H, 4.12; N, 13.69. DSC T_m = 141˚C.

2-((anthracen-9-yl)methylene)malononitrile (5)

Red powder. **Yield:** 71%. **^{1}H NMR (400 MHz, $CDCl_3$) δ** 8.95 (s, 1H), 8.66 (s, 1H), 8.10 (d, *J* = 8.4 Hz, 2H), 7.93 (d, *J* = 8.8 Hz, 2H), 7.71 – 7.65 (m, 2H), 7.62 – 7.56 (m, 2H). **^{13}C NMR (100 MHz, $CDCl_3$) δ** 160.70, 132.60, 131.02, 129.65, 129.21, 128.45, 126.17, 124.00, 123.51, 113.12, 111.51, 92.45. **FT-IR** (KBr, *v*, cm^{-1}): 3056 (C-H aromatic); 2229 (-C≡N), 1621 (C=C); 1575 (C-C stretching in the aromatic ring); 1211 (C-N stretching); 722 (C-N

deformation). **Anal. Calcd** for $C_{18}H_{10}N_2$ (254.29 g/mol): C, 85.02; H, 3.96; N, 11.02; Found: C, 85.08; H, 4.18; N, 11.00. DSC T_m = 213˚C.

2-((phenanthren-9-yl)methylene)malononitrile (6)

Yellow powder. **Yield:** 75%. **^{1}H NMR (400 MHz, $CDCl_3$) δ** 8.77 (d, *J* = 8.1 Hz, 1H), 8.70 (d, *J* = 8.3 Hz, 1H), 8.64 (s, 1H), 8.48 (s, 1H), 8.02 (d, *J* = 7.9 Hz, 1H), 7.94 (d, *J* = 8.2 Hz, 1H), 7.85 – 7.77 (m, 2H), 7.75 – 7.67 (m, 2H). **^{13}C NMR (100 MHz, $CDCl_3$) δ** 158.65, 132.66, 131.37, 130.67, 130.26, 130.14, 128.84, 128.14, 128.08, 127.90, 126.76, 123.84, 123.53, 122.95, 113.72, 112.50, 85.97. **FT-IR** (KBr, *v*, cm^{-1}): 3029 (C-H aromatic); 2226 (-C≡N), 1613 (C=C); 1569 (C-C stretching in the aromatic ring); 1197 (C-N stretching); 689 (C-N deformation). **Anal. Calcd** for $C_{18}H_{10}N_2$ (254.29 g/mol): C, 85.02; H, 3.96; N, 11.02; Found: C, 85.08; H, 4.20; N, 11.03. DSC T_m = 204˚C.

2-((pyren-1-yl)methylene)malononitrile (7)

Orange powder. **Yield:** 61%. **^{1}H NMR (400 MHz, $CDCl_3$) δ** 8.91 (s, 1H), 8.82 (d, *J* = 8.3 Hz, 1H), 8.38 – 8.32 (m, 3H), 8.31 – 8.24 (m, 3H), 8.16 – 8.11 (m, 2H). **^{13}C NMR (100 MHz, $CDCl_3$) δ** 156.46, 135.98, 131.58, 131.33, 131.30, 130.92, 130.58, 127.96, 127.66, 127.52, 127.20, 126.04, 125.35, 124.89, 124.35, 124.08, 121.31, 114.59, 113.44, 83.40. **FT-IR** (KBr, *v*, cm^{-1}): 3039 (C-H aromatic); 2220 (-C≡N), 1582 (C=C); 1560 (C-C stretching in the aromatic ring); 1198 (C-N stretching); 711 (C-N deformation). **Anal. Calcd** for $C_{20}H_{12}N_2$ (280.32 g/mol): C, 85.69; H, 4.31; N, 9.99; Found: C, 85.60; H, 4.03; N, 9.61. DSC T_m = 248˚C.

3. Result and discussion

3.1. Synthesis and characterization

The designed aromatic hydrocarbons bearing a dicyanovinylene unit, whose chemical structure is presented in Fig. 1, were synthesized via Knoevenagel reaction of aromatic aldehydes with malononitrile [$C_2H(CH)_2$]. In the condensation reaction aluminum oxide was used as a dehydrating agent. The compounds were obtained in good yield above 70%, except for 2-((pyren-1-yl)methylene)malononitrile (61%).

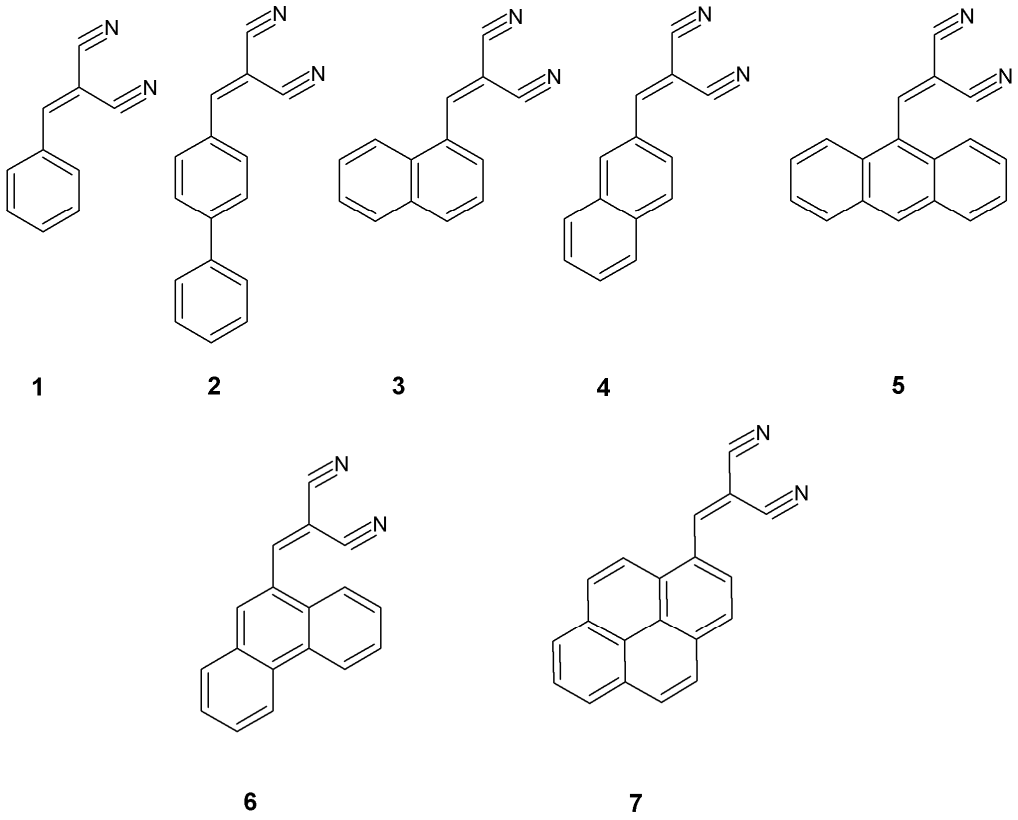

Fig. 1. Structures of the synthesized malononitrile derivatives.

The chemical structures of the prepared compounds and their purity were confirmed by instrumental techniques including ^{1}H NMR, ^{13}C NMR, FTIR and elemental analysis, respectively. The position of signals typical for protons in dicyanovinylene units depended on the molecular structure. For the compounds with phenyl (**1**) and biphenyl (**2**) units the signal of the vinyl proton was found at 7.78 ppm. The presence of condensed aromatic rings caused downfield shift of the proton signals. The largest down-field shift of the vinyl proton signals at 8.95 ppm and 8.91 ppm was observed in the compounds with anthracene (**5**) and pyrene (**7**), respectively. In the case of the molecules with naphthalene units (**3** and **4**), these signals depended on the substitution position of aromatic part with dicyanovinylene unit. In the molecule with naphthalene-1 (**3**), the vinyl proton signal was down field shifted to 8.66 ppm in comparison with that of the molecule with naphthalene-2 group (**4**), which was found at 8.29 ppm (cf. Supplementary Material Fig. S1). The shifts the proton signal confirmed the differences in conjugation in the synthesized push-pull molecules. Conjugation of electrons is more effective in molecules with condensed aromatic rings, with higher degree of conjugation present in the compound with anthracene unit (**5**) compared with the ones bearing phenylene rings (**1**,**2**). On the other hand the observed shift of the vinyl proton can be also associated with a decrease in electron density due to steric interactions between the vinyl proton and the

aromatic rings. In ^{13}C NMR spectra, the signals in the range of 156.46 - 160.70 ppm and 82.12 - 92.45 ppm confirmed the presence of carbon atom in vinyl units, and carbon atom bonded to cyano groups in the vinyl units, respectively. Signals in the range of 111.51 -113.44 ppm are characteristic for carbon in -C≡N groups (cf. Supplementary Material Fig. S1). The absorption of -C≡N groups in FTIR spectra was detected in the range of 2220 – 2228 nm. The elemental analysis results confirmed the purity of the obtained compounds. The photographs of **1**-**7** under daylight are presented in Supplementary Material Fig. S2.

3.2. Thermal properties

Differential scanning calorimetry (DSC) and thermogravimetric analysis (TGA) were applied to estimate the thermal behavior of the prepared compounds. The obtained data are collected in Table 1, whereas the representative DSC and TGA thermograms are given in Supplementary Material Fig. S3 and Fig. S4.

Table 1. Thermal properties of the investigated malononitrile derivatives.

Code	TGA			DSC (I run)	DSC (II run)
	T_5 [a] [°C]	T_{10} [a] [°C]	T_{max} [b] [°C]	T_m [c] [°C]	T_m [c] [°C]
1	137	153	191	88 (~86[23],~88[25,26])	87
2	225	245	294	144 (~140[27])	145
3	179	205	256	170 (~171[23],~163[28])	171
4	217	238	294	141 (~139[28])	142
5	225	236	282	213 (~212[23],~209[29])	213
6	242	260	308	204 (~203[23])	204
7	289(>400[21])	302	341	248 (~254[23])	249

[a] T_5, T_{10} - temp. based on 5%, 10% weight loss from TGA curves. [b] Temp. of the maximum decomposition rate from DTG curves. [C] Melting temp. registered upon I and II a heating scan.

All of the compounds showed crystalline nature and their melting points (T_m), detected as endotherms in DSC thermograms registered under the first heating run, depend on the chemical structure of the molecule. The compound with the phenylene unit (**1**) melted at the lowest temperature, and increase of the aromatic rings being condensed, caused increase of the melting temperature values. However, the thermal properties also depend on the substitution position of the aromatic ring with dicyanovinylene unit. In the case of molecules with naphthalene structure (**3** and **4**), higher T_m was detected for the compound, in which the dicyanovinylene group was attached to the naphthalene ring in α position (**3**), in comparison with the one being substituted in ß position (**4**). In the compounds with three condensed aromatic rings, i.e. with anthracene (**5**) and phenanthrene (**6**) units, higher T_m was detected for

the example with the anthracene moiety. The compound (**7**), which contains four condensed aromatic rings, melted at the highest temperature. During cooling DSC scan exothermic peak indicated crystallization of the compounds was seen. The second DSC heating scan, after cooling, showed only melting endotherm. Thermogravimetric analysis gave information about temperatures, in which the compounds start to decompose (T_5), detected as the temperature values of 5% weight loss. It was found that the molecules with anthracene (**5**) and α-naphthalene (**3**) units start to decompose about 10 degrees beyond their melting points. On the contrary, the molecule with ß-naphthalene unit (**4**) starts to decompose about 70 degrees over its melting temperature. Also a big difference between melting and decomposition temperatures - about 80 degrees - was observed in the compound with biphenyl unit (**2**). About 40 degrees difference between melting and decomposition temperatures was found for the compound with phenanthrene (**6**) and pyrene (**7**) units.

3.3. Electrochemical properties

The electrochemical properties were investigated in CH_2Cl_2 by means of cyclic voltametry (CV) using glassy carbon electrode as the working electrode. The cyclic voltamograms of **2**,**4**,**6** and **7** are presented in Fig. 2.

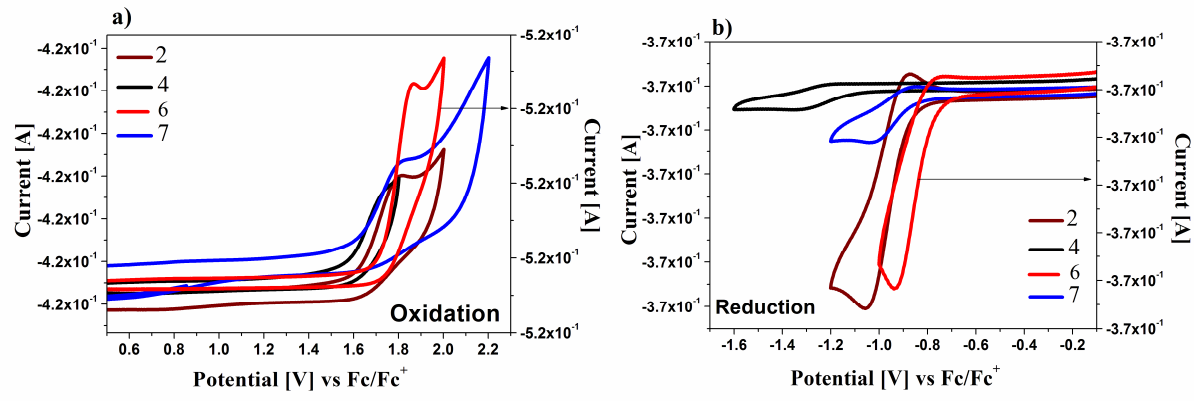

Fig. 2. Cyclic voltammograms of **2**,**4**,**6** and **7** during a) oxidation and b) reduction process (GC; scan rate 0.100V·s^{-1}; c = 10^{-4} mol/dm^3; 0.2 M Bu_4NPF_6 in dichloromethane).

The electrochemical reduction and oxidation onset potentials were used for estimating ionization potentials (IP) and electron affinities (EA) of the compounds (IP of ferrocene equals -5.1 eV according to [30]). The calculated EA and IP levels, together with electrochemical energy band gap (E_g), are presented in Table 2.

Table 2. Electrochemical parameters (CV), IP and EA together with HOMO and LUMO and the energy band gaps.

Code	$E_{ox\ onset}^{CV}$ [V]	E_{ox}^{CV} [V]	IP^{CV} [eV]	$E_{red\ onset}^{CV}$ [V]	E_{red}^{CV} [V]	EA^{CV} [eV]	E_g^{CV} [eV]	$HOMO^{DFT}$ [eV]	$LUMO^{DFT}$ [eV]	E_g^{DFT} [eV]
1	1.18	1.73	-6.28	-0.92	-1.14	-4.18	2.10	-6.93	-2.78	4.16
2	1.62	1.81	-6.72	-0.88	-1.05	-4.22	2.50	-6.41	-2.81	3.59
3	1.50	1.75	-6.60	-0.84	-1.02	-4.26	2.34	-6.27	-2.82	3.45
4	1.31	1.74	-6.41	-1.05	-1.31	-4.05	2.36	-6.31	-2.79	3.52
5	1.32	1.44	-6.42	-0.87	-1.03	-4.23	2.19	-5.70	-2.79	2.91
6	1.72	1.85	-6.82	-0.77	-0.93	-4.33	2.49	-6.18	-2.71	3.48
7	1.55	1.78	-6.65	-0.85	-1.03	-4.25	2.40	-5.74	-2.75	2.99

$IP(eV) = (-5.1 - E_{ox\ onset}) \cdot |e|$. $EA(eV) = (-5.1 - E_{red\ onset}) \cdot |e|$. $E_g^{CV} = E_{ox\ onset} - E_{red\ onset}$. E_g^{DFT} = HOMO – LUMO.

The malononitrile derivatives with aromatic rings were electrochemically active. Based on the difference between peaks potentials (ΔE_p) the irreversible reduction process for **1** (ΔE_p above 300 mV, cf. Fig. S12) and the *quasi*-reversible process for other compounds (ΔE_p about 150 mV) was seen. In the reduction process, the 2,2-dicyanovinyl (-CH=C(CN)$_2$) as electron deficient moiety was involved [1, 2, 24, 31]. The lowest and the highest $E_{red\ onset}$ were observed for the molecules with phenanthrene (**6**) and β-naphthyl structure (**4**), respectively (cf. Table 2). Slight differences in reduction (~ 0.28 – 0.38 V) and larger differences in the oxidation (~ 0.41 – 0.54 V) potentials were noted. The oxidation process is related to the donor substituent attached to the vinylene bond [1, 2, 24, 31]. Similar values of $E_{ox\ onset}$ for compounds with anthracene (**4** and **5**) were observed, where it would be expected to obtain similar potentials for **3** and **4** due to similar chemical structures. Based on the $E_{ox\ onset}$ it can be concluded that compound **1** exhibits the strongest electron-donating ability (i.e. $E_{ox\ onset}$ at a lowest potential than for **2-7**). Paramaguru and et al. [21] carried out electrochemical measurements for **7** (with pyrene), obtaining the oxidation potential at 1.66 V. The difference in the obtained potentials can be due to different solvents and methods (in [21] DMF solution and DPV method were used).

The compounds exhibited the nature of n-type semiconductors, having a low LUMO orbital (EA below 4.0 eV) [32]. The calculated energy band gap (E_g) was in the range 2.10 - 2.50 eV, being the lowest for **1** (with phenyl) and the highest for **2** (with biphenyl). Low energy band gap values, below 3.00 eV, make it possible to use **1-7** compounds in optoelectronic devices [32, 33].

3.4. Geometric structures and frontier molecular orbitals

Theoretical calculations were performed with the use of the density functional theory (DFT) and were carried out using the Gaussian09 program [34] on B3LYP/6-31g++ level [35, 36]. Molecular geometry of the singlet ground state of the compounds was optimized in the gas phase and their electronic structures, electronic transitions, and first and second singlet excited states were calculated with the Polarizable Continuum Model (PCM) in chloroform as a solvent. Such calculations were carried out for analysis of the frontier molecular orbitals structure and energy levels, UV-Vis and photoluminescence data. The optimized geometries of **1**-**7** are depicted in Fig. S5 in the Supplementary Material, and Fig. S6 presents experimental and calculated IR spectra. The molecules (**1**) and (**4**) are planar in ground and S_1, S_2 excited states and in the case of other ones a methylene malononitrile fragment is bent at an angle of about 30° to 54° in ground state. In the first and second excited states the angle between arene and dicyanovinylene (–HC=C(CN)$_2$) grows up to 90° in the case of compound (**5**) (cf. Table S1 in Supporting Materials). The biphenyl part in the 2-((1,1'-biphenyl)-4-yl-methylene)malononitrile molecule (**2**) in the S_1 state is more planar than in ground state with the relatively small deformation of the biPh-CH=C(CN)$_2$ plane. Similarly, in the case of **3** the molecule in the S_1 state is significantly flatter than in S_0. However, the molecule **7** in the second excited state is more planar than in ground state. Generally, in the excited states the methylene C=C bond is extended by about 0.1 Å, the C-CN bonds are shortened by about 0.02 Å and C≡N distance increases by about 0.01 Å (cf. Table S1 in Supporting Materials).

Based on the optimized geometries, next the frontier molecular orbitals of the compounds were analyzed. Comparing the energies of HOMOs and LUMOs determined on the basis of electrochemical data with theoretically obtained values (cf. Table 2), it can be seen that calculated HOMO energies are compatible with the experimental values of ionization potentials determined from CV measurements. The largest difference of 0.91 eV occurs for compound (**7**). On the other hand, calculated LUMO energies are much higher than those determined experimentally. The virtual orbitals are generally harder to be described theoretically than the occupied ones [37], however, the calculated values of the HOMO and LUMO energies were used only for consistency with geometry optimization. For a more detailed description of the molecular orbitals, the contributions of parts i.e. arene and dicyanovinyl fragments to a molecular orbital, were calculated. The obtained DOS diagrams are depicted in Fig. S7 and composition of selected molecular orbitals in ground as well as first and second excited states are gathered in Tables S2-S4 in Supplementary Material.

HOMO and LUMO comprise the whole molecule, although, except (**1**), aromatic hydrocarbons play a dominant role in HOMO, whereas LUMO is dominated by π^* orbitals of $-CH=C(CN)_2$ fragment. The lower energy occupied orbital HOMO-1 and higher energy LUMO+1 are localized on the aromatic, i.e. phenyl, biphenyl, α-naphthyl, β-naphthyl, anthracene, phenanthrene and pyrene, fragment of the molecules. The compounds are polar in the ground and in the excited S_1, S_2 states compounds (**1-4**) have dipole moments greater and (**5-7**) lower than in the ground state, although the changes of the dipole moments are small (cf. Table S1).

3.5. Electronic absorption and fluorescence characteristics

UV-vis absorption and photoluminescence (PL) spectra of the hydrocarbons with dicyanovinylene unit were registered in two solvents with different dielectric constants, i.e. chloroform (ε = 4.81) and NMP (ε = 33.0) at the same concentration equal to 10^{-5} mol/L and in solid state as well. Additionally, the UV-Vis spectra of the compounds were calculated with the use of the TD-DFT [38] method (cf. Fig. S8 in Supplementary Materials). The electronic absorption spectra registered in chloroform solution are presented in Fig. 3 and spectroscopic data, that is, positions of maximum absorption band (λ_{max}) with value of molar absorption coefficient are collected in Table 3.

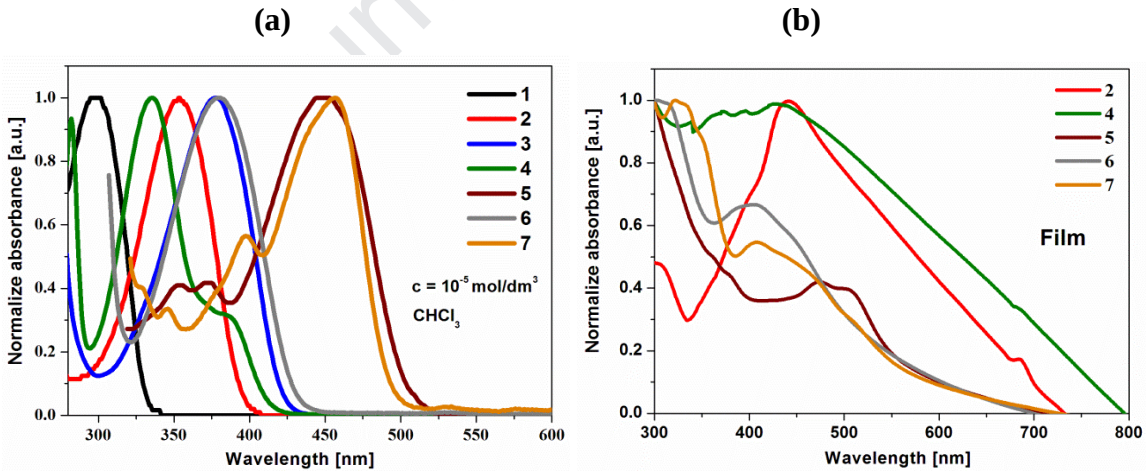

Fig. 3. Normalized UV-vis spectra of the compounds in (a) $CHCl_3$ and (b) film on glass substrate.

The UV-vis absorption spectra of the compounds consist of two bands located below and above 300 nm. According to the calculations, the lowest absorption band corresponds to the $S_0 \rightarrow S_1$ (HOMO→LUMO) transition and, based on the data collected in Table S2 and DOS diagrams shown in Fig. S7, the transition can be followed by charge decrease in the aromatic

part of the molecules and charge increase on the dicyanovinylene fragment. Thus, the mixed intramolecular charge transfer/locally-excited (ICT/LE) nature of the S_1 state is evident.

The bathochromic shift of λ_{max} according to aromatic part structure was detected (cf. Fig. 3a.). The molecules with anthracene (**5**) and pyrene (**7**) units absorbed radiation in the lower energy range. Similar absorption range was found for the compounds with α-naphthyl (**3**) and phenanthrene (**6**) unit. Replacement of α-naphthalene (**3**) structure with biphenylene (**2**) hypsochromically shifted λ_{max} from 377 to 352 nm.

In the case of compounds with the condensed aromatic rings absorption bands at longer wavelengths in less polar solvent - chloroform was bathochromically shifted (**3** - **7**) in comparison with the ones in NMP. However, the shift for the compounds with naphthalene and pyrene (**7**) moieties was very small and was found to be 8 nm for the molecule with α-naphthalene unit (**3**), 3 nm for the one with ß-naphthalene moieties (**4**), and 12 nm for the one with pyrene (**7**) structure. In the case of the compound with anthracene (**5**), the negative solvatochromism was more pronounced. The investigated malononitrile derivatives in NMP exhibited higher value of molar absorption coefficient indication better light harvesting ability than in chloroform solution. The light harvesting efficiency (LHE) in chloroform solution was calculated using equation LHE = $1\text{-}10^{-f}$, where *f* is the oscillator strength of the compound [20] and the highest value 0.83 exhibited molecule with pyrene unit (**7**).

Electronic spectra were also taken for films cast from chloroform. In all cases absorption bands of the film were observed at longer wavelengths than in the $CHCl_3$ solution for the same compound (cf. Fig. 3b). It was not possible to detected λ_{max} for the compound with phenyl (**1**) and α-naphthalene unit (**3**), because the absorption bands were broad without any the structured maximum.

All prepared malononitrile derivatives were fluorescent in solution and in solid state as film and powder, emitting radiation with maximum emission band (λ_{em}) in the range of 390 - 609 nm (cf. Table 3). The representative PL spectra are depicted in Fig. 4a,b.

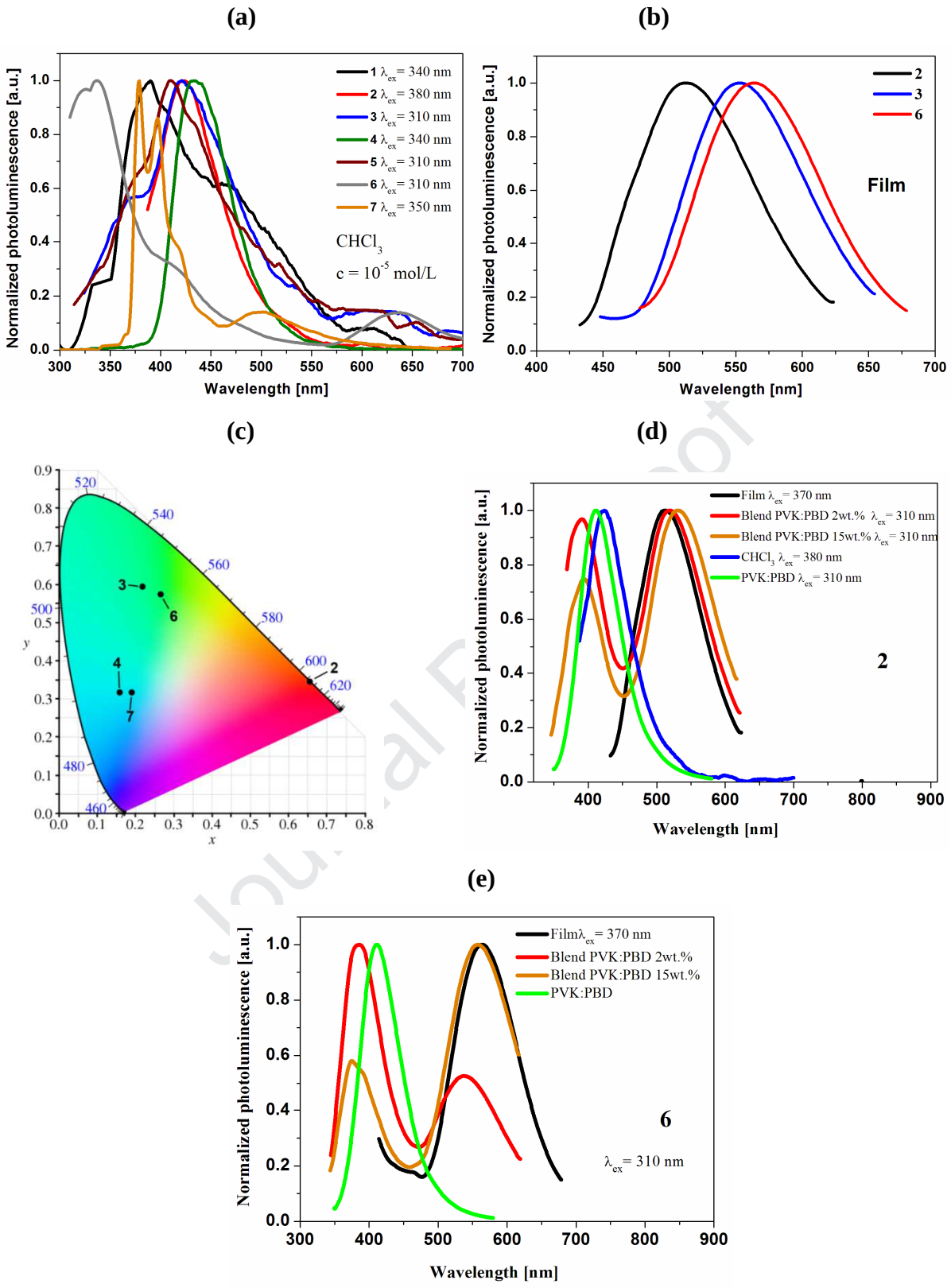

Fig. 4. PL spectra (a) of all compounds in $CHCl_3$, (b) **2**,**3** and **6** as film, (c) powders chromaticity plots (CIE 1931), (d) **2** and (e) **6** in $CHCl_3$, film, blend PVK:PBD 2wt.% / 15wt.% with PL of PVK:PBD.

All of the compounds showed more intense PL in chloroform than in the NMP solution. Table S5 contains calculated electronic transitions corresponding to excitations resulting in the most intense luminescence intensity in chloroform solution. The excitation of **5-7** compounds occurs at wavelengths corresponding to low intensity (cf. Fig. S8), which are connected to $S_0 \rightarrow S_2$ transition. Considering that H-2/H-2/HOMO and LUMO/L+1 are involved in these transitions, it can be concluded that S_2 state has also ICT/LE character. Moreover, the molecular structure of **7** in S_2 state is more planar than in S_1, thus the second excited state of this compound definitely prevails LE character. In PL spectra of molecules **1-5** one emission band located in blue spectral range was noted. Whereas the fluorescence spectra of **6** and **7** in chloroform solution show two emission bands (cf. Table 3 and Fig. 4a), one intense band in UV region and the second weak band with maximum at 632 nm and 500 nm for **6** and **7**, respectively. The first one originates from the $S_2 \leftarrow S_0$ transition and the weak, low intensity one in the visible region arises from $S_1 \leftarrow S_0$ transition. The $S_2 \leftarrow S_0$ fluorescence may appear if the $S_2 \leftarrow S_1$ radiationless internal conversion process is sufficiently slow. This situation can happen when the energy gap between S_2 and S_1 levels is large enough. It is assumed that the energy gap greater than $\Delta E > 3000$ cm^{-1} reduces the vibronic coupling between these states and slows the rate of the $S_2 \leftarrow S_1$ internal conversion processes [39]. Calculated value of the energy gap between the S_1 and S_2 states (**7**) is equal to 5965 cm^{-1} and is sufficiently large for the observation of the S_2 emission. In the case of **6** the energy gap between second and first excited state of 1675 cm^{-1}, which indicates the possibility of the conversion process and the emission bands from the S_1 and S_2 states are not separated although the intensity of the long–wave band is definitely lower. In the case of **5** the conversion process seems to be probable because the energy difference between the second and first excited states is small (595 cm^{-1}), therefore only one emission band originating from the $S_1 \leftarrow S_0$ transition is observed. Moreover, the energy difference between S_1 and S_0 states of **5** corresponds well to the fluorescence maximum (experimental 416 nm, calculated 412 nm). We also considered the possibility that the low intensity band at lower energies is the result of $T_1 \leftarrow S_0$ transition. However, the energy difference between excited and ground states: $S_1 \leftarrow S_0$ 614 nm, $S_2 \leftarrow S_0$ 450 nm and $T_1 \leftarrow S_0$ 1010 nm calculated for compound **7** indicate probability of the $S_2 \leftarrow S_0$ emission for compounds **6** and **7**.

Table 3. UV–Vis electronic and photoluminescence data of the compounds (in solution c = 10^{-5} mol/dm^3).

Code	Medium	UV-vis	PL				
		λ_{max} [nm] ($\varepsilon \cdot 10^{-4}$)[a]	λ_{ex}[nm]	λ_{em}[nm]	Stokes shift [cm^{-1}][b]	Φ [%]	LHE
1	$CHCl_3$	309 (4.2)	340	390	6721	0.5	-
	NMP	311^{sh} (2.3)	350	420	-	-	-
	Film	nd	310	**373**;500^{sh}	-	1.7	-
	Powder	-	340	383	-	-	-
2	$CHCl_3$	352 (9.6)	380	424	4824	1.4	-
	NMP	352 (24.9)	380	448	6088	-	-
	Film	440	370	513	3234	8.2	-
	Powder	-	510	609	-	-	-
	PVK:PBD[c]	-	310	388,**520**	-	3.4,4.8	-
	PVK:PBD[d]	-	310	392,**531**	1664	4.4,5.1	-
3	$CHCl_3$	267 (9.8), 377 (9.9)	310 377	418 -	2602 -	1.5 -	- 0.55
	NMP	262 (8.9), 369 (8.2)	310	358	-	-	-
	Film	nd	340	552	-	2.1	-
	Powder	-	470	549	-	-	-
4	$CHCl_3$	282 (11.0), 334 (11.7) 384* (3.8)	340 384	434 -	6899 -	1.2 -	- 0.41
	NMP	281 (9.2), 331 (11.4) 384* (4.7)	310	**364**,455^{sh}	-	-	-
	Film	428	350	490	2956	3.1	-
	Powder	-	360	493	-	-	-
5	$CHCl_3$	249 (21.1), 280 (3.1) 449 (1.8)	310 449	416 -	- -	2.2 -	- 0.58
	NMP	349 (1.9) , 370 (1.7), 430 (2.8)	370	471	-	-	--
	Film	473, 503	310	**363**,530	-	6.8,2.2	-
6	$CHCl_3$	252 (10.7), 380 (2.5)	310 380	**330**,632 -	- -	1.3 -	- 0.12
	NMP	270 (4.5), 289 (1.9), 300 (1.8), 370 (4.1)	310	370	-	-	-
	Film	312, 402	310 370	563 **563**	- 7114	- 7.9	- -
	Powder	-	490	555	-	-	-
	PVK:PBD[c]	-	310	**384**,538	-	5.3,3.6	-
	PVK:PBD[d]	-	310	373,**557**	-	2.7, 6.6	-
7	$CHCl_3$	265^{sh} (4.9), 311 (2.4) 345 (0.9), 394 (1.5) 454 (2.6)	350 450	**378**, 500 -	- -	5.2,0.5 -	- 0.83
	NMP	278 (0.5), 311 (2.4) 345* (1.2), 394 (2.0) 442 (2.9)	350	395	-	-	-
	Film	319, 405	nd	nd	-	-	-
	Powder	-	410	495	-	-	-

[a] **ε** - Absorption coefficient, [dm^3·mol^{-1}·cm^{-1}]. ^{sh} – shoulder. Bold data indicates the most intense PL.
[b] Stokes shifts calculated according to the equation $\Delta v=(1/\lambda_{abs}-1/\lambda_{em})\cdot 10^7$ [cm^{-1}].
* the second derivatives method was used. Nd – not detected.
[c] 2wt% concentration of the compound in PVK:PBD (50wt%:50wt%).
[d] 15wt% concentration of the compound in PVK:PBD (50wt%:50wt%).

Maxima of the emission for all the compounds in the solid state were bathochromically shifted in comparison with the ones in $CHCl_3$ solution (except for **1** and **7**). IEC chromaticity diagram is presented in Fig. 4c. Compounds as powders emitted in the UV range (**1**) and in the visible range (**2**, **3**, **4**, **6**, **7**). Compound with biphenyl unit (**2**) was emissive in the red range, with α- naphthyl (**3**) and phenanthrene (**6**) unit in the green range, and ß- naphthyl (**4**) and pyrene (**7**) unit in the blue range. Photoluminescence quantum yield (Φ_{PL}) of the compounds in $CHCl_3$ solution was found to be in the range of 0.5 - 5.2 %. The highest values were detected for the compound with pyrene structure (**7**). The malononitrile derivatives showed higher Φ_{PL} in film than in the solutions. This behavior can be assigned to the aggregation induced emission phenomena (AIE) [40,41]. Taking into account the compound structure, one can see that the presence of biphenyl unit (**2**) resulted in the increase of PL yield in comparison with the molecule with phenyl unit (**1**) in solution and in the film. Film of the compound with ß - naphthyl unit (**4**) exhibited higher PL quantum yield than the one with α- naphthyl moiety (**3**). In the case of the compounds with three condensed aromatic rings, PL yield the film of the molecule with phenanthrene (**6**) unit was higher than the value of the film prepared from the molecule with anthracene unit (**5**).

3.6. Electroluminescence performance

The electroluminescence (EL) ability of the selected malononitrile derivatives was tested in a guest-host type diode. A binary matrix consisting of poly(9-vinylcarbazole) (PVK (50 wt. %)) and 2-(4-start-butylphenyl)-5-(4-biphenylyl)-1,3,4-oxadiazole (PBD (50 wt. %)) as hole and electron transport layers was used, respectively. Two compounds with biphenyl (**2**) and phenanthrene (**6**) unit were molecularly dispersed with content 2 or 15 wt.% in a matrix to form the active layer in the device. These molecules were selected based on PL spectra in blend with PVK:PBD. In the case of these blends intense band ascribed to the photoluminescence of **2** and **6**, except of band originating from the emission of the matrix, was observed (cf. Fig. 4d,e and Fig. S9). The presence of emission of PVK:PBD suggests no complete energy transfer from the host to the guest, which can be expected considering UV-Vis absorption range of studied malononitrile derivatives [1,42]. Energy transfer can take place via Förster (FRET) or Dexter processes in the guest-host system. FRET can take place when the emission spectrum of the host overlap with the absorption spectrum of the luminophore [1,2,43,44]. For series of the investigated compounds only partial overlap was

seen (cf. Fig. S10). Diodes with structure ITO/PEDOT:PSS/PVK:PBD:**compound**/Al were fabricated.

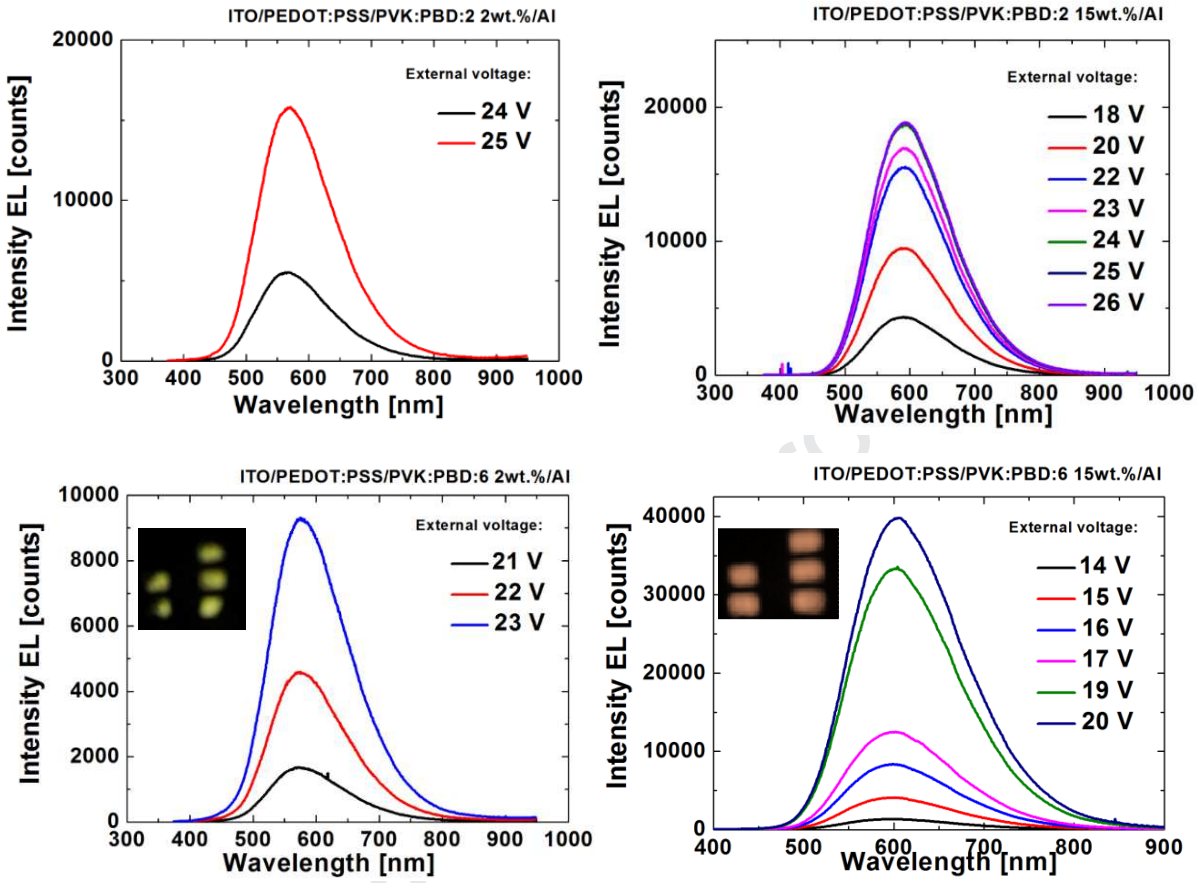

Fig. 5. The electroluminescence spectra of prepared OLED.

The prepared diodes showed EL with maximum emission band (λ_{EL}) located in range of 569-604 nm. Increasing the compounds content in a matrix from 2 to 15 wt.% revealed the red shift of λ_{EL} and increase of the EL intensity.

3.7. Photovoltaic performance

Photovoltaic performance of selected malononitrile derivative with pyrene unit (**7**), which exhibited the highest LHE, was tested in DSSC. It was found that tetracyanate units were used as anchoring groups in several organic dyes applied in DSSC [45]. Thus, it could be expected that dicyanovinylene units may anchor molecules to TiO_2 surface. However, the lack of anchoring ability of –CN group with TiO_2 was demonstrated [20,46] and confirmed in our study. Nevertheless in the presented investigations a mixture of a commercial bis(4,4'-dicarboxylato-2,2'-bipyridine)-bis(isothiocyanoto)ruthenium(II) (N719) (cf. Fig. S11) with 2-((pyren-1-yl)methylene)malononitrile (**7**) was applied for anode preparation. As reference

photoanode with only N719 was prepared. Considering the UV-Vis spectra of N719, **7** and mixture of N719 with **7** in solution (Fig. 6a) the enhancement of absorption ability in the range of 350-500 nm of mixture in comparison with N719 was observed.

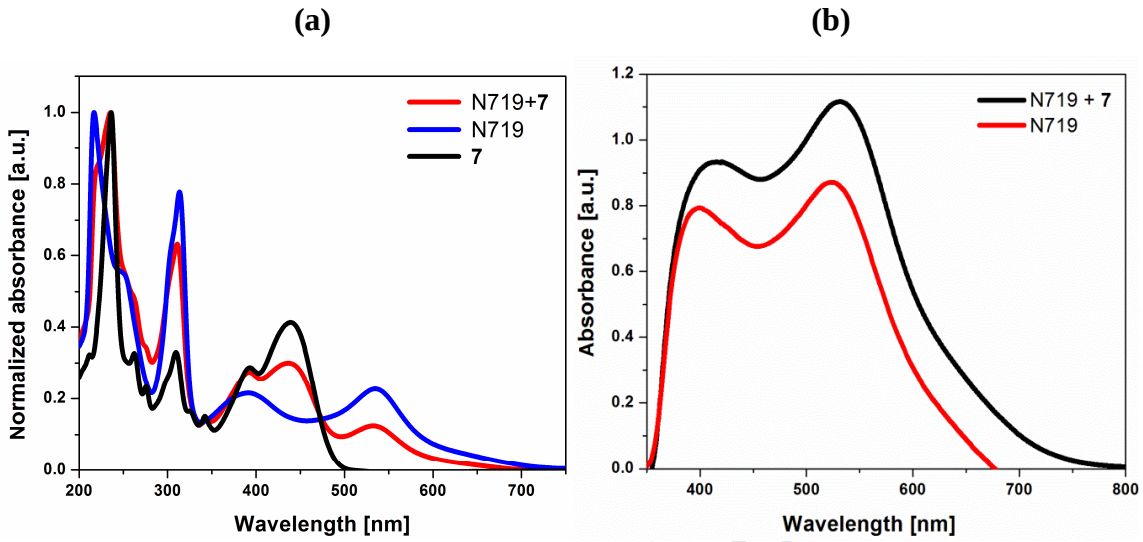

Fig. 6. The UV-Vis spectra of (a) **7**, N719 and its mixture in ACN: t-butyl alcohol solution ($c = 3 \cdot 10^{-5}$ mol/dm^3) and (b) TiO_2 with adsorbed dyes after 48 h immersion in solution.

The absorption band of substrate TiO_2 contains two dyes was characterized with higher absorbance and wider absorption range compared with N719 (cf. Fig.7b). The AFM measurements showed that the TiO_2 with adsorbed dye was more planar, as indicated by root-mean square (RMS) roughness values (cf. Fig. 7). RMS of the photoanodes was found to be 86, 52, 55 nm for TiO_2 without dye, with N719, N719+**7** mixture, respectively.

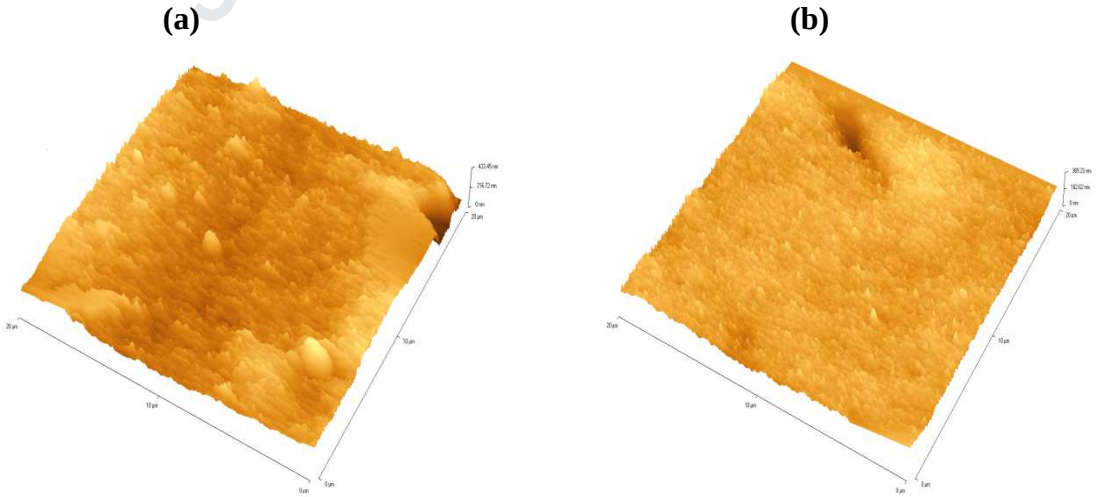

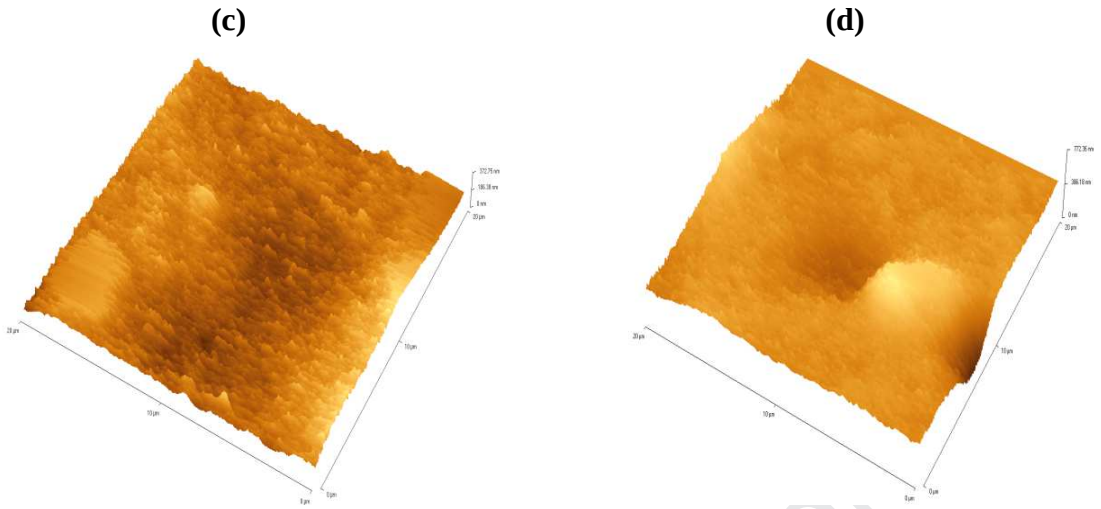

Fig. 7. The AFM micrographs of the surface TiO_2 (a) without dye, (b) with adsorbed dyes mixture (**7** and N719), (c) with adsorbed N719 (c = 3 x 10^{-5} mol/dm^3) and (d) with adsorbed N719 (c = 1.5 x 10^{-4} mol/dm^3).

The DSSC device with photoanode prepared from the mixture of **7** with N719 was fabricated. Additionally, the reference cell based on N719 was constructed. Based on registered the current density – voltage (J-V) characteristics of prepared cells, the photovoltaic parameters, such as short circuit current (J_{SC}), open circuit voltage (V_{OC}), fill factor (FF) and power conversion efficiency (PCE) were calculated. It was found that both types of devices exhibited similar photovoltaic parameters (cf. Table 4).

Table 4. Photovoltaic parameters of prepared DSSCs.

Code	V_{oc} [mV]	J_{sc} [mA/cm^2]	FF [-]	PCE [%]
Device with N719	747	19.64	0.46	6.84
Device with N719*	731	14.84	0.39	4.28
Device with N719+7	726	18.18	0.50	6.78

* photoanode prepared from N719 solution with concentration 1.5 · 10^{-5} mol/ dm^3.

DSSC with photoanode prepared with a neat N719 showed J_{SC}, V_{OC}, FF and PCE equal to 19.64 mA/cm^2, 747 mV, 0.46 and 6.84%, respectively. On the other hand, the device in which photoanode was immersed in the mixture of N719 with **7** exhibited J_{SC}, V_{OC}, FF and PCE equal to 18.18 mA/cm^2, 726 mV, 0.50 and 6.78%, respectively. Thus, it can be concluded that using compound **7** as coadsorbent, the reduction of N719 amount can be achieved while keeping similar photovoltaic performance. The concentration of solution used for photoanode preparation with N719 and dyes mixture was 3.0 x 10^{-4} mol/dm^3. Thus, in the case of device

with dyes mixture half less amount of N719 was applied. In order to confirm the impact of **7** on PV performance, the photoanode with N719 using its solution with concentration of 1.5 x 10^{-4} mol/dm^3 was prepared. Device based on such electrode was denoted as N719*. As can be seen from Table 4 such a cell exhibited significantly lower PCE as compared to the others. The lower efficiency resulted mainly from the low value of FF, which may be a consequence of photoanode surface quality. RMS of the photoanode prepared from lower concentration N719 solution was 73 nm, being higher compared to other electrodes (cf. Fig. 8d). The more uniform and smooth photoanode surface may be owing to the filling of some pores with dye molecules, giving a boost the PV parameters [47]. The presented results showed a significant effect of compound **7** on the photovoltaic parameters of the cell with photoanode obtained from a mixture of the dyes.

4. Conclusions

Summarizing the presented results it can be concluded that:

- all malononitryle derivatives except for 2-((phen-1-yl)methylene)malononitrile showed relevant thermal properties required for compounds for organic electronics,
- the presence of anthracene (**5**) and pyrene (**7**) moiety significantly shifted absorption range to lower energy region. Substitution of naphthalene unit at α-position with dicyanovinylene (**3**) bathochromically shifted λ_{max} compare to compound with β-naphthyl (**4**),
- all investigated compounds were fluorescent in solid state and emitted red (**2**), green (**3** and **6**) and blue (**4** and **7**) light as well as radiation with λ_{em} around 360 nm (**1** and **5**). The highest quantum PL yield about 8% exhibited films obtained from malononitrle derivatives containing biphenyl (**2**) and phenanthrene unit (**6**),
- based on PL spectra of malononitrle derivatives dispersed molecularly in matrix (PVK:PBD) the most efficient, however not complete, energy transfer from host to luminophore was observed in the case of molecules with biphenyl (**2**) and phenanthrene unit (**6**),
- the constructed diodes with structure ITO/PEDOT:PSS/PVK:PBD:**2**or**6**/Al emitted light with λ_{EL} in range of 569 - 604 nm, however, these compounds seems to be rather poor candidates for real OLED applications,

- the utilization of 2-((pyren-1-yl)methylene)malononitrile (**7**) for photoanode preparation allowed decreased by half of N719 amount, practically without sacrificing DSSC performance.

Acknowledgments

Funding: This work was supported by the National Science Centre of Poland Grant No. 2016/23/B/ST8/02045. The GAUSSIAN-09 calculations were carried out in the Wrocław Centre for Networking and Supercomputing, WCSS, Wrocław, Poland, http://www.wcss.wroc.pl (grant number 18).

Authors thank to Dr. Henryk Janeczek for DSC measurements.

REFERENCES

[1]Kotowicz S., Sęk D., et al (2018) Malononitrile derivatives as push-pull molecules: structure - properties relationships characterization, J. Lumin., 203:455 – 466.
[2]Sęk D., Kotowicz S., et al. (2019) Thermal, spectroscopic, electrochemical, and electroluminescent characterization of malononitrile derivatives with triphenylamine structure, Spectro. Acta A: Mol. Biol., 210:136 – 147.
[3]Bernede J.C., Cattin L., Morsil M., et al (2012) Improvement of the efficiency of organic solar cells using the terthiophene-pyran-malononitrile (T3PM) as electron donor, through the use of a MoO_3/CuI anode buffer layer, Energy Procedia., 31: 81 – 88.
[4]Dhondge A.P., Chen J.-Y., Lin T., et al (2018) Di-2-(2-oxindolin-3-ylidene)malononitrile Derivatives for N-type Air-Stable Organic Field-Effect Transistors, 20:40 – 43.
[5]Jayalakshmi L. N., Karuppasamy, A., Stalindurai K., et al. (2015) A Mechanochemical Approach for the Construction of Carbon–Carbon Double Bonds: Efficient Syntheses of Aryl/Heteroaryl/Aliphatic Acrylates and Nitriles, Catal. Lett., 145: 1322 – 1330.
[6]Kühbeck D., Saidulu G., Reddy K. R., Diaz D. D. (2012) Critical assessment of the efficiency of chitosan biohydrogel beads as recyclable and heterogeneous organocatalyst for C–C bond formation, Green Chem., 14, 2012, 378 – 392.
[7]Qiao Y., Zhang L., Li J., et al (2016) Switching on Supramolecular Catalysis via Cavity Mediation and Electrostatic Regulation, Angew. Chem., 128:12970 – 12974.
[8]Johansson K.-J., Andreae M. R. M., Berkessel A., Davis P. A. (2005) Organogel media for on-bead screening in combinatorial catalysis, Tetrahedron Lett., 46:3923 – 3926.
[9]Gruttadauria M., Bivona L. A., Lo Meo P., Riela S., Noto R. (2012) Sequential Suzuki/Asymmetric Aldol and Suzuki/Knoevenagel Reactions Under Aqueous Conditions, Eur. J. Org. Chem., 2012, :2635 – 2642.
[10]Ma L., Wang X., Deng D., et al (2015) Five porous zinc(ii) coordination polymers functionalized with amide groups: cooperative and size-selective catalysis, J. Mater. Chem. A, 3:20210 – 20217.
[11]Shinobu W., Suzuki H. (2003) Calcite and fluorite as catalyst for the Knövenagel condensation of malononitrile and methyl cyanoacetate under solvent-free conditions, Tetrahedron Lett., 44, 2003, 399 – 401.

[12]Kaupp G., Naimi-Jamal M. R., Schmeyers J. (2003) Solvent-free Knoevenagel condensations and Michael additions in the solid state and in the melt with quantitative yield, Tetrahedron, 59, 2003, 3753 – 3760.
[13]Watts W. P., Haswella S. J., Pombo-Villar E. (2005) The preparation and reaction of carbanions within micro reactors, Tetrahedron 61:10757 – 10773.
[14]Zhao J., Lin B., Zhu Y., Zhou Y., Liu H. (2018) Phosphor-doped hexagonal boron nitride nanosheets as effective acid–base bifunctional catalysts for one-pot deacetalization–Knoevenagel cascade reactions, Catal. Sci. Technol., 8: 5900 – 5905.
[15]He H., Sun F., Aguila B., et al (2016) A bifunctional metal–organic framework featuring the combination of open metal sites and Lewis basic sites for selective gas adsorption and heterogeneous cascade catalysis, J. Mater. Chem. A, 4:15240 – 15246.
[16]Lin Q., Chen P., Fu Y.-P., et al (2013) A green synthesis of a simple chemosensor that could instantly detect cyanide with high selectivity in aqueous solution, Chin. Chem. Lett., 24:699 – 702.
[17]Turpaev K., Ermolenko M., Cresteil T., Drapier J. C. (2011) Benzylidenemalononitrile compounds as activators of cell resistance to oxidative stress and modulators of multiple signaling pathways. A structure–activity relationship study, Biochem. Pharmacol., 82:535 – 547.
[18]Krishnamoorthy G., Asato A. E., Liu R. (2003) Conformational isomerizations of symmetrically substituted styrenes. No-reaction photoreactions by Hula-twist, Chem. Commun, 17:2170 – 2171.
[19]Jiang L., Fu Y., Li H., Hu W. (2008) Single-Crystalline, Size, and Orientation Controllable Nanowires and Ultralong Microwires of Organic Semiconductor with Strong Photoswitching Property, J. Am.Chem. Soc., 130: 3937 – 3941.
[20]Kathiravan A., Panneerselvam M., Sundaravel K., et al (2016) Unravelling the effect of anchoring groups on the ground and excited state properties of pyrene using computational and spectroscopic methods, Phys. Chem. Chem. Phys., 18:13332 – 13345.
[21]Paramaguru G. , Rajadurai V. S., Sivanadanam J., et al. (2013) Effect of electron withdrawing anchoring groups on the optoelectronic properties of pyrene sensitizers and their interaction with TiO_2: A combined experimental and theoretical approach, J. Photochem. Photobiol. A:, 271: 31 – 44.
[22]Breffke J., Williams B. W., Maroncelli M. (2014) The Photophysics of Three Naphthylmethylene Malononitriles, J. Phys. Chem. B, 119:9254–9267.
[23]Katritzky A. R., Zhu D. W., Schanze K. S. (1991) Intramolecular charge transfer properties of dicyanovinyl-substituted aromatics, J. Phys. Chem., 95:5737–5742.
[24]Szłapa A., Kula S., Błaszkiewicz U., et al. (2016) Simple donor–π–acceptor derivatives exhibiting aggregation-induced emission characteristics for use as emitting layer in OLED, Dyes Pigmt., 129:80–89.
[25]Qiao L., Cai Y., Yao H., et al (2015) A colorimetric and fluorescent cyanide chemosensor based on dicyanovinyl derivatives: Utilization of the mechanism of intramolecular charge transfer blocking, Spectro. Acta A: Mol. Biol.: 136: 1047-1051.
[26]Jayalakskmi L.N., Karuppasamy A., Stalindurai K., et al (2015) A Mechanochemical Approach for the Construction of Carbon–Carbon Double Bonds: Efficient Syntheses of Aryl/Heteroaryl/Aliphatic Acrylates and Nitriles, Catalysis Letters: 145:1322-1330.
[27]Matsuoka M., Takao M., Kitao T., et al (1990) Cyanovinylheteroaromatics for Organic Nonlinear Optics, Mol. Crys. Liq. Crys. Incorp. Nonlin. Opt., 182: 71-79.
[28]Madasamy K., Kumaraguru S., Sankar V., Mannathan S., Kathiresan M. (2019) A Zn based metal organic framework as a heterogeneous catalyst for C–C bond formation reactions, New J. Chem., 43:3793-3800.

[29]Noroozi P., Kimia M.A., Jalilzadeh M., Sahin E. (2013) A New, Fast and Easy Strategy for One-pot Synthesis of Full Substituted Cyclopropanes: Direct Transformation of Aldehydes to 3-Aryl-1,1,2,2-tetracyanocyclopropanes, J. Chin. Chem. Soc., 60: 35 – 44.
[30]Bujak P., Kulszewicz-Bajer I., Zagorska M., et al (2013) Polymers for electronics and spintronics, Chem. Soc. Rev.,42:8895–999.
[31]Kotowicz S., Kula S., et al (2018) 2,2-Dicyanovinyl derivatives – Thermal, photophysical, electrochemical and electroluminescence investigations, Mater. Chem. Phys., 209: 249 – 261.
[32]Li Y., Sonar P., Murphy L., Hong W. (2013) High mobility diketopyrrolopyrrole (DPP)-based organic semiconductor materials for organic thin film transistors and photovoltaics, Energy Environ. Sci., 6:1684 – 1710.
[33]Świst A., Sołoducho J. (2012) Organiczne półprzewodniki - materiały przyszłości?, CHEMIK, 66, 2012, 289 – 296.
[34]Gaussian 09, Revision A.02, Frisch M. J., Trucks G. W., Schlegel H. B., Scuseria G. E., Robb M. A., Cheeseman J. R., Scalmani G., Barone V., Petersson G. A., Nakatsuji H., Li X., Caricato M., Marenich A., Bloino J., Janesko B. G., Gomperts R., Mennucci B., Hratchian H. P., Ortiz J. V., Izmaylov A. F., Sonnenberg J. L., Williams-Young D., Ding F., Lipparini F., Egidi F., Goings J., Peng B., Petrone A., Henderson T., Ranasinghe D., Zakrzewski V. G., Gao J., Rega N., Zheng G., Liang W., Hada M., Ehara M., Toyota K., Fukuda R., Hasegawa J., Ishida M., Nakajima T., Honda Y., Kitao O., Nakai H., Vreven T., Throssell K., Montgomery J. A. Jr., Peralta J. E., Ogliaro F., Bearpark M., Heyd J. J., Brothers E., Kudin K. N., Staroverov V. N., Keith T., Kobayashi R., Normand J., Raghavachari K., Rendell A., Burant J. C., Iyengar S. S., Tomasi J., Cossi M., Millam J. M., Klene M., Adamo C., Cammi R., Ochterski J. W., Martin R. L., Morokuma K., Farkas O., Foresman J. B., and D. J. Fox, Gaussian, Inc., Wallingford CT, 2016.
[35]Becke A. D. (1993) Density-functional thermochemistry. III. The role of exact exchange., J.Chem.Phys. 98:5648-5652.
[36]Lee C., Yang W., Parr R.G. (1988) Development of the Colle-Salvetti correlation-energy formula into a functional of the electron density, Phys. Rev. B 37: 785-789.
[37]Zhang G., Musgrave Ch. B. (2007) Comparison of DFT Methods for Molecular Orbital Eigenvalue Calculations, J. Phys. Chem. A, 111: 1554-1561.
[38]Casida M. E., in: J. M. Seminario (Ed.), Recent Developments and Applications of Modern Density Functional Theory, Theoretical and Computational Chemistry, vol. 4, Elsevier, Amsterdam, 1996, p.391.
[39]Mondal J. A., Ghosh H. N., Mukherjee T., Palit D. K. (2005) S_2 Fluorescence and Ultrafast Relaxation Dynamics of the S_2 and S_1 States of a Ketocyanine Dye, J. Phys.Chem. A, 109:6836-6846.
[40]Jung M. – H., Song K.H., et al (2010) Nonvolatile memory organic field effect transistor induced by the steric hindrance effects of organic molecules, J. Mater. Chem., 20:8016 – 8020.
[41]Zhao Q., Sun J. Z., Red and near infrared emission materials with AIE characteristics, J. Mater. Chem. C, 4:10588 – 10609.
[42]Hussain S.A., An introduction to fluorescence resonance energy transfer (FRET), arXiv: 0908.1815, 2009.
[43]Kotowicz S., Kula S., et al (2018) 2,2-Dicyanovinyl derivatives – Thermal, photophysical, electrochemical and electroluminescence investigations, Mater. Chem. Phys., 209:249 – 261
[44]Qu B., Chen Z., et al (2009) Full-color OLEDs based on conjugated materials, Front. Optoelectron. China, 2:92 – 102.

[45] Zhang L., Jacqueline M. C. (2015) Anchoring Groups for Dye-Sensitized Solar Cells, ACS Appl. Mater. Interfaces,7:3427−3455.
[46] Paramaguru G., Rajadurai V. S., Sivanadanam J. et al (2013) Effect of electron withdrawing anchoring groups on the optoelectronic properties of pyrene sensitizers and their interaction with TiO_2: A combined experimental and theoretical approach, J. Photochem Photobiol. 271:31-44.
[47] Atli A., Atilgan A., Yildiz A. (2018) Multi-layered TiO2 photoanodes from different precursors of nanocrystals for dye-sensitized solar cells, Sol Energy., 173:752–758.

> Seven aromatic hydrocarbons bearing a dicyanovinyl unit were prepared. > The effect of chemical structure on their properties was demonstrated. > All investigated compounds were fluorescent in solid state. >The selected compounds were tested in OLED and dye-sensitized solar cells. > The using of **7** let to decreased by half of N719 amount without sacrificing DSSC performance. >

As a corresponding author of the paper (DYPI_2020_487) entitled *"Photoelectrochemical and thermal characterization of aromatic hydrocarbons substituted with dicyanovinylene unit"* (S. Kotowicz, D. Sęk, S. Kula, A. Fabiańczyk, J. G. Małecki, P. Gnida, S. Maćkowski, M. Siwy, E. Schab-Balcerzak), I sent the revised version of this manuscript.

Ewa Schab-Balcerzak

Declaration of interests

☒ The authors declare that they have no known competing financial interests or personal relationships that could have appeared to influence the work reported in this paper.

☐The authors declare the following financial interests/personal relationships which may be considered as potential competing interests: